

Unified analysis of spatially-coupled absorption and saturation dynamics in multi-pass pumped thin-disk lasers

HANJIN JO,^{1,*} JIŘÍ MUŽÍK,¹ PAWEŁ SIKOCINSKI,¹ MAGDALENA SAWICKA-CHYLA,¹ MICHAL CHYLA,¹ YUYA KOSHIBA,¹ YOANN LEVY,¹ KOHEI HASHIMOTO,¹ MARTIN SMRŽ,¹ AND TOMÁŠ MOCEK¹

¹*HiLASE Centre, Institute of Physics of the Czech Academy of Sciences, Za Radnicí 828, 252 41 Dolní Břežany, Czech Republic*

*hanjin.jo@hilase.cz

Abstract: We present a theoretical framework that unifies pump absorption, gain saturation, thermo-optic distortion, and cavity diffraction into a self-consistent model of multi-pass pumped solid-state lasers. By deriving a theoretical formulation of the nonlinear coupling of the superimposed pump energy and effective absorption, we prove an unique steady-state solution exists. Applied to the multi-pass Yb:YAG thin-disk module, the framework is quantitatively validated with experiments, reproducing a well matched absorption tendency, errors in output power, beam diameter and M^2 within 3.0%, 1.7%, and 0.05 respectively. This approach provides predictive guidelines for pump-power scaling and pass-number optimization in high-power lasers.

1. INTRODUCTION

High-power solid-state lasers involve complex energy transfer between optical fields and gain media, where thermal and mechanical deformations of the optical elements strongly influence cavity dynamics [1–6]. Traditionally, laser output has been estimated by evaluating the population inversion derived from steady-state energy transfer equations. The conventional approach typically compresses diverse loss mechanisms into single effective terms and underestimating pump-beam distributions with approximate saturation effects. However, it is crucial to consider the coupled dynamics of pump absorption, saturation of gain and pump, and thermally influenced active media in high power regime [7–11]. While the prediction of signal power is sufficient from the energetics point of view, it is essential to accurately define the spatially overlapped pump energy when extending the model to two-dimensional (2D) intra-cavity optical fields. Moreover, a precise evaluation of the pump absorption is essential to theoretically derive the deformation of the medium and its effect on intra-cavity optical field evolution.

To address these limitations, we derive the absorbed pump power per pass in a self-consistent mathematical framework, extended to 2D intra-cavity fields. The formulation produces a unique fixed-point solution valid from single-pass to infinite-pass geometries, accounting for spatially accumulated energy, temperature-dependent cross-sections, and nonlinear saturation effects, which efficiently yield the pump-beam intensity distribution in the gain medium prior to reaching stimulated emission of the signal beam. To the best of our knowledge, this study presents the first comprehensive approach integrating spatial deformation, thermal effects, absorption, and emission of the medium as interdependent factors.

The formulation was first validated experimentally by measuring the unabsorbed parts from the Yb:YAG thin-disk module. Then, it is applied to the Yb:YAG laser system by combining measured disk optical path difference (OPD) maps with the rate equation to describe the cavity dynamics. The derived effective pump intensity with consideration of the medium temperature reproduces the absorption, signal power, beam quality and diameters in the experiment, demonstrating quantitative agreement with high-power resonator behavior.

2. MATERIALS AND METHODS

2.1. Theoretical approach

The core of our approach is a self-consistent equation in which the locally accumulated pump energy and the effective absorption coefficient are determined simultaneously, fully coupling absorption-, gain-saturation, thermal effects, and spatial intensity distributions. Assuming monochromatic pumping into a medium of thickness L and cross-sectional area A_p , we define the steady-state effective absorption coefficient α_{eff} by equating the local pump-photon flux to the rate of ground-state depletion under steady-state rate equations. If saturation intensity is not considered, the absorption rate must be re-evaluated based on the signal oscillating within the cavity dynamics. Since this approach consumes significant resources in 2D field calculations, it is substantially efficient to derive the effective pump intensity when it is not lasing.

Saturation arises from changes in the level of population densities: stimulated emission depletes the excited-state while ground-state absorption depletes the ground-state [12, 13]. Because both processes act on the same atomic ensemble, any change in upper-state population that controls output power must concurrently affect pump absorption—even when the transitions occur at different wavelengths. Thermalization of the quantum-defect energy further alters line-widths, cross-sections and population distributions, reinforcing this mutual coupling [14, 15]. The absorption dynamics of Yb:YAG can be adequately described by a two-level system since rapid intra-manifold thermal relaxation instantaneously equilibrates the electronic population within each of the $^2F_{7/2}$ and $^2F_{5/2}$ manifolds. Here, excited-state absorption, cross relaxation and energy transfer upconversion are neglected due to the nature of ytterbium ion [16, 17]. At the steady-state temperature T_{ss} , α_{eff} is defined with saturation intensity in pump wavelength $I_{\text{sat}}^{(p)}$ and pump intensity I_p as follows.

$$\alpha_0 = N_0 \sigma_{\text{abs}}^{(p)}(T_{\text{ss}}), \quad \alpha_{\text{eff}} = \frac{\alpha_0}{1 + I_p / I_{\text{sat}}^{(p)}} \quad (1)$$

where $N_0 = N_1 + N_2$, total ion density, τ_f is the fluorescence lifetime, and $\sigma_{\text{abs}}^{(p)}(T_{\text{ss}})$ is the absorption cross-section at T_{ss} . Eq. (1) is called the absorption saturation effect derived from the population inversion equation (See Supplement 1.A), and effectively captures the reduction in the absorption rate induced by population inversion. In the steady-state response, the effective absorption α_{eff} must follow

$$\frac{\partial \alpha_{\text{eff}}}{\partial t} = 0, \quad (0 \leq \alpha_{\text{eff}} \leq \alpha_0) \quad (2)$$

The saturation intensity for the pump and signal wavelength (p, l) ,

$$I_{\text{sat}}^{(p,l)} = \frac{h\nu^{(p,l)}}{(\sigma_{\text{abs}}^{(p,l)}(T_{\text{ss}}) + \sigma_{\text{em}}^{(p,l)}(T_{\text{ss}}))\tau_f} \quad (3)$$

If one measures cross-section values, it inherently includes Stark-manifold averaging and re-absorption/re-emission corrections, which obviates the need for explicit modeling of individual Stark sublevels. Alternatively, one can derive theoretical values [8]. Note that, if only the absorption saturation effect is considered, the absorption saturation intensity should be derived based on the absorption cross-section. A uniform pumping energy $E_0 = \int P_0 dt$ per pass is transmitted and spatially overlapped on each traversal, yields the total overlapped energy E_{OL} after n_{pass} passes,

$$\begin{aligned}
E_{\text{OL}} &= E_0 e^{-\alpha_{\text{eff}} L} \sum_{k=0}^{n_{\text{pass}}-1} e^{-k \alpha_{\text{eff}} L} \\
&= E_0 e^{-\alpha_{\text{eff}} L} \frac{1 - e^{-n_{\text{pass}} \alpha_{\text{eff}} L}}{1 - e^{-\alpha_{\text{eff}} L}}
\end{aligned} \tag{4}$$

Simultaneously, the effective pump intensity I_{eff} is defined with spatially overlapped energy and cross-sectional area A_p , which is ($I_{\text{eff}} = dE_{\text{OL}}/A_p dt = I_p$). The pump intensity in the gain media depends on the number of passes and on the evolution of the local absorption coefficient α that is considered as effective over one pass. This absorption coefficient itself depends on the local intensity of the pump and on the number of the pass. To find the α_{eff} , a self-consistent equation must therefore be solved. The self-consistent equations Eq. (5) is derived by Eqs. (4) and (1), under steady-state response.

$$f(\alpha_{\text{eff}}, I_{\text{eff}}) = \frac{\alpha_0}{1 + \frac{I_{\text{eff}}}{I_{\text{sat}}} \frac{e^{-\alpha_{\text{eff}} L} (1 - e^{-n_{\text{pass}} \alpha_{\text{eff}} L})}{(1 - e^{-\alpha_{\text{eff}} L})}} \tag{5}$$

It highlights that the effective pump intensity and effective absorption coefficient α_{eff} follow uniquely from a steady-state self-consistent formulation. The self-consistent equation is a non-linear equation, and the absorption rate does not change in a steady-state while pumping the gain medium. From Eq. (5), α_{eff} satisfies

$$\alpha_{\text{eff}} = f(\alpha_{\text{eff}}, I_{\text{eff}}) \tag{6}$$

The mapping $f(\alpha_{\text{eff}}, I_{\text{eff}})$ is continuous on the closed interval $[\varepsilon, \alpha_0]$ and satisfies $f([\varepsilon, \alpha_0], I_{\text{eff}}) \subseteq [\varepsilon, \alpha_0]$. Moreover, $f(\alpha_{\text{eff}}, I_{\text{eff}})$ is strictly decreasing in α , with $f(0, I_{\text{eff}}) > 0$ and $f(\alpha_0, I_{\text{eff}}) < \alpha_0$. By the intermediate value theorem, there exists a fixed point $\alpha_{\text{eff}}^* \in (0, \alpha_0)$ such that $f(\alpha_{\text{eff}}^*, I_{\text{eff}}) = \alpha_{\text{eff}}^*$. Monotonicity guarantees its uniqueness. Hence, one finite self-consistent pair $(\alpha_{\text{eff}}^*, I_{\text{eff}})$ exists for each $I_{\text{eff}} > 0$ (See Supplement 1.B for the detailed proof).

Under the uniform-field approximation, the absorbed pump intensity is obtained by integrating the local absorption rate

$$\frac{P_{\text{abs}}}{A_p} = \int_0^L \alpha(z) I(z) dz \approx \alpha_{\text{eff}} I_{\text{eff}} L \tag{7}$$

so that $\alpha_{\text{eff}} I_{\text{eff}}$ denotes the local absorbed pump power density ($\text{W} \cdot \text{m}^{-3}$). From Eq. (1), the absorbed power density is

$$\begin{aligned}
\mathcal{A}(I_{\text{eff}}) &\equiv \alpha_{\text{eff}} I_{\text{eff}} = \frac{\alpha_0 I_{\text{eff}}}{1 + I_{\text{eff}}/I_{\text{sat}}} \\
&= \alpha_0 I_{\text{sat}} \frac{x}{1 + x} \quad \text{where} \quad x \equiv \frac{I_{\text{eff}}}{I_{\text{sat}}}
\end{aligned} \tag{8}$$

which increases monotonically with I_{eff} and tends to the finite limit $\alpha_0 I_{\text{sat}}$ as $x \rightarrow \infty$. Hence, although $\alpha_{\text{eff}} \rightarrow 0$ for very large I_{eff} , the absorbed power density does not vanish but saturates; the absorbed power per unit area tends to $\alpha_0 I_{\text{sat}} L$ in the uniform field approximation.

In the low-absorption limit ($\alpha_{\text{eff}} L \ll 1$ i.e. low pumping intensity), admits a Taylor expansion whose leading term yields the familiar linear scaling (Eq. (8)) reduces to the linear approximation

$$I_{\text{eff}} \approx \frac{P_0}{A_p} n_{\text{pass}} (1 - \alpha_0 L) \tag{9}$$

which validates the expressions employed in our analysis of multi-pass pumping [8–10]. In the limit $I_{\text{eff}} \gg I_{\text{sat}}$ (i.e., when the incident pump power is much larger than the saturation intensity or, equivalently, when the absorption cross section is very small), Eq. (8) reduces to

$$I_{\text{eff}} \approx \frac{P_0}{A_p} \times n_{\text{pass}} \quad (10)$$

Since achieving the condition of ($I_{\text{eff}} \gg I_{\text{sat}}$) is unattainable for the gain media of interest and practically undesirable, it is essential to derive a self-consistent pair ($\alpha_{\text{eff}}^*, E_{\text{OL}}^*$). If we assume $n_{\text{pass}} \rightarrow \infty$, the E_{OL} in the medium can be defined as Eq. (11).

$$\lim_{n_{\text{pass}} \rightarrow \infty} E_{\text{OL}} = \frac{E_0 e^{-\alpha_{\text{eff}} L}}{1 - e^{-\alpha_{\text{eff}} L}} \quad (11)$$

Assuming a large number of passes, it is proper to derive the self-consistent pair ($\alpha_{\text{eff}}^*, E_{\text{OL}}^*$) through Eqs. (11) and (1). Fig. 1(a) shows the experimental setup used to measure the unabsorbed pump beam in the 32 pass Yb:YAG thin-disk module. As seen in Fig. 1(b), the difference in effective pump intensity between relatively low and high incident intensities is clearly observed. The derived ($\alpha_{\text{eff}}^*, E_{\text{OL}}^*$) demonstrate their effectiveness in the high-intensity pumping regime.

Pump photon flux (Φ_p) is derived by effective pump intensity $\Phi_p = I_{\text{eff}}/h\nu^{(p)}$. Pump photon flux, reflecting pump saturation effect and estimated Gaussian order shown in Fig.2(a), replaces the usual single-pass intensity in the quasi-three level rate equation defined by inversion ratio $\beta = N_2/N_0$. For quasi-three level media such as Yb:YAG, where the lower laser level lies near the ground-state and rapidly decays to it, thermal excitation partially repopulates the lower level, allowing a quasi-three level approximation [18].

$$\begin{aligned} \frac{d\beta}{dt} = & -\gamma_{12}\beta + [(\sigma_{\text{abs}}^{(p)}(1-\beta) - \sigma_{\text{em}}^{(p)}\beta)\Phi_p \\ & + (\sigma_{\text{abs}}^{(l)}(1-\beta) - \sigma_{\text{em}}^{(l)}\beta)\Phi_l] \end{aligned} \quad (12)$$

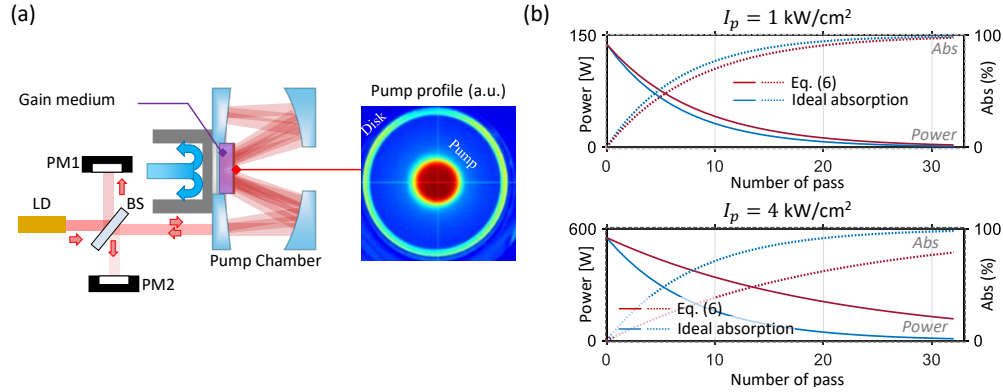


Fig. 1. (a) experimental configuration of measuring unabsorbed power measurement. (b) Typical calculation results of the absorption behavior with (Eq. (6)) and without saturation effects (Ideal absorption) for pump intensities of 1 kW/cm² and 4 kW/cm². Note pump intensity I_p is defined as the incident pump power divided by the pump beam area. Pump beam radius is 2.05 mm. Abbreviations are following; LD: laser diode, PM: power-meter and BS: beam splitter.

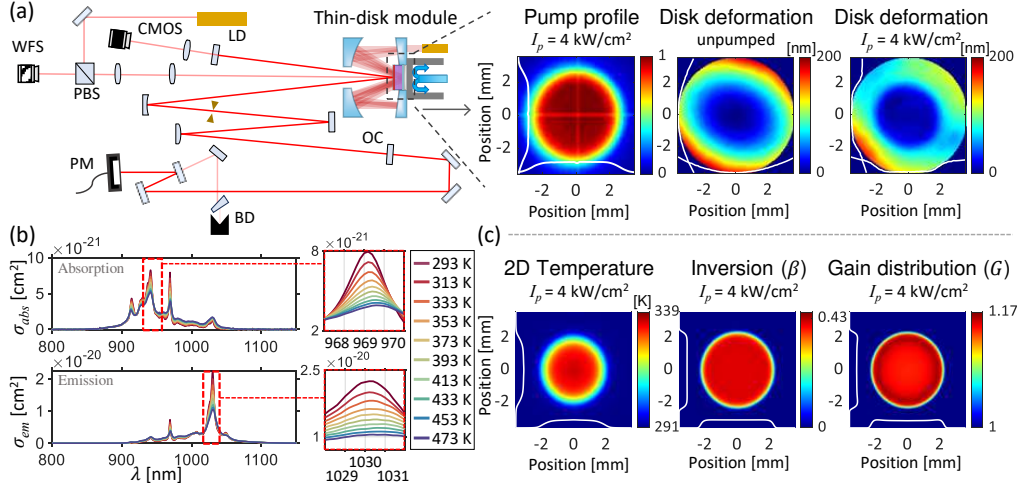


Fig. 2. (a) Experimental setup: simultaneous measurement of output power, disk wavefront during pumping. Typical example has been shown for the pump intensity of 4 kW/cm² (b) Temperature-dependent absorption and emission cross-section of Yb:YAG. (c) Typical example of simulated 2D distributions: temperature, inversion, and gain when pumping intensity of 4 kW/cm². Abbreviations as follows; WFS: wavefront sensor, LD: laser diode, PM: power-meter, BD: beam dump, PBS: polarized beam splitter and OC: output coupler.

where $\gamma_{12} = 1/\tau_f$ is the decay rate and Φ_l is signal photon flux $\Phi_l = I_l/h\nu^{(l)}$. Eq. (12) ensures that gain saturation, temperature dependent cross-sections, and spatial pump beam distribution are all captured. The absorption and emission cross-sections used in this equation are measured values corresponding to T_{ss} , as shown in Fig. 2(b). The I_{eff} is utilized for deriving pump photon flux, then small signal gain g_0 is derived via β

$$g_0(\beta) = N_0(\sigma_{em}^{(p,l)}\beta - \sigma_{abs}^{(p,l)}(1 - \beta))$$

$$G_D(\beta) = e^{(g_{eff}L)} \quad (13)$$

The intra-cavity signal photon flux (Φ_l) can be derived with effective small signal gain $g_{eff} = g_0/(1 + I_l/I_{sat}^{(l)})$, then used for deriving gain factor G_D . In our framework, the atoms participating in pump absorption and those contributing to stimulated emission are drawn from the same population, ensuring a consistent treatment of absorption and gain saturation. Rather than iteratively solving for absorption equilibrium within each field propagation step, we employ gain saturation to implicitly capture pump depletion. The resulting performance closely matched experimental observations, demonstrating the predictive power of the self-consistent model.

2.2. Roundtrip propagation

The derived photon flux is utilized to determine the precise distribution of the electric field $u(x, y)$ inside the cavity. The intra-cavity optical field arises from repeated amplification, diffractive propagation, and superposition of emissions the source [19, 20]. Thus, we assume single-unpolarized beams seeded by spontaneous emission. We chose the convenient seed term as $u_{in}(x, y) = u_{SE}(x, y)$, a spatially localized spontaneous emission source. For segment j of distance d_j , the combined propagation operator \mathcal{P}_j includes the Rayleigh–Sommerfeld diffraction \mathcal{R}_j and complex phase \mathcal{M}_j of the optics.

$$\mathcal{P}_j\{u(x, y)\} \equiv \mathcal{M}_j \circ \mathcal{R}_j\{u(x, y)\} \quad (14)$$

The disk-induced phase difference is defined in terms of the total surface profile $S_{D,\text{tot}}(x, y)$ and the vacuum wavenumber k_0 as

$$\mathcal{M}\{S_{D,\text{tot}}\} = e^{-i \cdot 2k_0 \cdot S_{D,\text{tot}}} = e^{-i\Psi_D} \quad (15)$$

where Ψ_D is the OPD of the disk, capturing the effects of mechanical, thermal-expansion, and air convection, which are naturally accounted for the diffraction calculation [20, 21]. The surface deformation has been considered via factor 2 due to the reflection. The measured disk surface has been utilized for the disk-induced phase (see Fig. 2(a)). Composing the segment operators gives the round-trip operator \mathcal{T}

$$\mathcal{T}\{u(x, y)\} \equiv \mathcal{P}_N \circ \mathcal{P}_{N-1} \circ \dots \circ \mathcal{P}_2 \circ \mathcal{P}_1\{u(x, y)\} \quad (16)$$

After the k -th disk encounter the field is updated as

$$u_k(x, y) = u_{SE}(x, y) + \sqrt{\alpha_l \cdot G_D(x, y)} e^{[-i\Psi_D(x, y)]} \mathcal{T}\{u_{k-1}(x, y)\} \quad (17)$$

($k = 1, 2, \dots$)

where α_l is total intra-cavity loss including transmission of the output coupler 5% with cavity losses 1%. The circulating power after converging within the numerical tolerance represents $(\Delta P/\bar{P} < 0.001)$, $u_k(x, y)$ represents the steady-state intra-cavity field prior to output coupling. The intra-cavity field $u_k(x, y)$ evolves sequentially, as shown in Fig. 3(a).

2.3. Experimental details and numerical implementation

We first validated the approach by measuring the unabsorbed pump power (Fig. 1(a)) and subsequently confirmed it in single mode laser by comparing predicted and measured 2D output fields (Fig. 2(a)). The experimental setup was used with a 7.9%-doped, 188 μm -thick Yb:YAG disk, with pump intensities from 0 to 4 kW/cm^2 . The reconstructed pump profile from measured one (estimated super Gaussian of order 6) and in-situ disk surface deformation were used as inputs, while all other optical components were treated as ideal (Fig. 2(a)). As shown in Fig. 2(b), measured absorption and emission cross-sections have been used [22], and applied to compute the initial 2D inversion and gain distributions (Fig. 2(c)). Temperature distribution of the disk was computed using COMSOL Multiphysics by considering pumping intensity distribution with complex structure of the disk (diamond heatsink, disk bonding layer, and active medium), and validated against measured surface temperatures (Teledyne FLIR A65). From the measured cross-sections and temperature maps, 2D inversion and local gain maps can be calculated (Fig. 2(c)). The fluorescence lifetime (τ_f) is set as 0.95 ms for Yb:YAG, which does not show significant changes depending on the temperature of the medium, as shown in previous reports [23, 24]. Beam diameter was evaluated according to the ISO 11146 standard and the M^2 parameter by deriving the covariance matrix [25, 26].

3. RESULTS AND DISCUSSION

In this research, we compared unabsorbed pump power by the simulation, then applied the effective pump intensity into the gain medium to derive the signal intensity. The error in the absorption rate is maximum 3% in 1 kW/cm^2 pump intensity region, and it shows a well matched

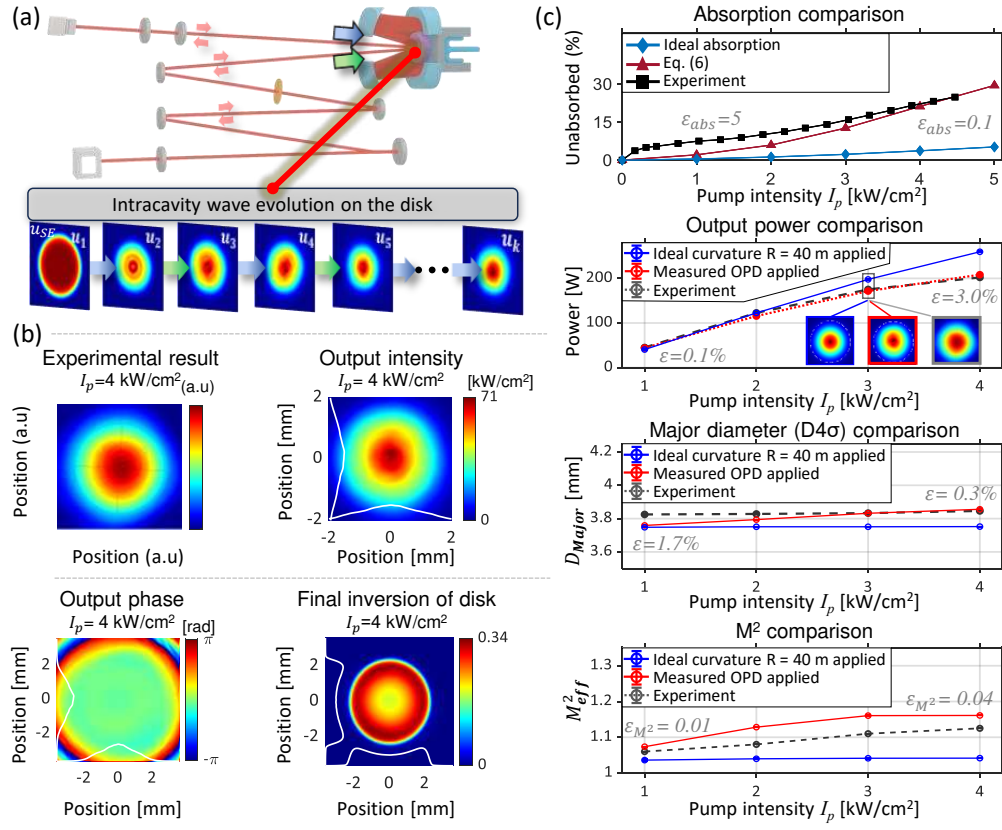


Fig. 3. (a) Representative example illustrating the evolution of the intracavity wave. (b) Typical example of the output beam, simulated beam profile, phase and the population inversion ratio of the disk in the steady state. (c) Summary of results: comparison between experiment and simulation, where a radius of curvature of 40 m obtained from the wavefront sensor was applied. Unabsorbed ratio, output power, major beam diameter (D_{maj}), and beam quality factor (M^2) are compared. Note, ε_{abs} is difference of unabsorbed ratio between the experiment and derived value from Eq. (6), ε is relative errors and ε_{M^2} absolute errors between the experiment and measured OPD applied simulation results.

tendency as shown in Fig. 3(c). To eliminate this fundamental error in the low pump intensity region, the calculation needs to be spectrally resolved based on the population inversion ratio (β). Fig. 1(b) exhibits notably high non-absorption at high pump intensities. Such a high residual pump transmission is not observed in practical laser operation, since at the signal resonance the population inversion is reduced and the effective absorption coefficient correspondingly increases. Nevertheless, the proposed method practically provides an initial value for the pump-photon flux, enabling prediction of signal power, which assumes the monochromatic pump and monochromatic signal.

Numerical calculations were carried out to account for the phase change induced by the gain medium, considering (i) the ideal disk curvature $R = 40 \text{ m}$ and (ii) the measured surface deformation. The resulting phase profiles were then (iii) validated against the experimental data. Fig. 3(a) shows intra-cavity field evolution for case (ii). As shown in Fig. 3(b), the field-based approach enables the evaluation of the steady-state field, phase, and population inversion of the disk. The simulation incorporating the measured deformation of disk yields markedly

improved agreement with experiment (Fig. 3(c)). Quantitatively, the numerical model reproduces output power within 3.0%, major and minor beam diameters within 1.7%, and M^2 within 0.05 of the measured values. The small errors further underscore the validity of this approach. This agreement validates the coupling of the derived self-consistency formula, rate-equation, and propagation equation in the processing of 2D optical fields.

The actual pump-photon flux in laser operation cannot be obtained from a simple estimation, because absorption and stimulated emission are dynamically coupled through the population inversion. The field must be updated in the transient-state and the corresponding effective absorption has to be calculated with amplified spontaneous emission (ASE), and temperature-dependent level populations. Moreover, single-mode operation typically involves a pumped area larger than the signal, producing spatial inversion inhomogeneity. Paradoxically, the substantial complexity of deriving an accurate population inversion further highlights the practical utility of the output predictions obtained with the method proposed here.

Two principal effects govern multi-pass performance in our configuration. First, effective pump intensity depends non-linearly on intensity and pass number because the steady-state absorption that enters the rate equation and the saturated gain that determines amplification are mutually coupled; this coupling places a hard constraint on local intensities and implies that improving efficiency requires either a medium with higher saturation intensity or greater pump overlap with higher absorption rate. Second, because the pump profile and all other optics are identical between cases, the $\approx 23\%$ reduction in achievable output at 4 kW/cm^2 pumping relative to the ideal-curvature ($R=40 \text{ m}$) simulation is attributable to diffraction arising from the measured disk deformation; this deformation is therefore the dominant source of mode mixing and output loss under the conditions tested. The errors in output power between the experiment and the simulation increase nonlinearly with pump intensity due to ASE, as previously reported [27], yet the resulting discrepancy remains small because ASE is generated inside the resonator and is effectively suppressed by the output coupler transmission. The experimental validation underscores the importance of optimizing the gain medium curvature and pump beam profile to realize the ideal disk geometry prerequisite for fundamental transverse mode operation.

4. CONCLUSION

We have developed and theoretically derived a self-consistent framework that couples temperature-dependent absorption and gain saturation with cavity diffraction dynamics. This theoretical approach effectively addresses the method for dealing with pump photon flux from low- to high-intensity regime. The framework shows high fidelity to experimental results, expanded into the cavity in 2D spatial domain. Applied to Yb:YAG, the framework reproduces the absorption rate, output power, beam size, and M^2 in excellent agreement with the experiment.

Funding. This research was co-funded by the European Union (MERIT - Grant Agreement No. 101081195) and European Union and the state budget of the Czech republic under the project LasApp CZ.02.01.01/00/22_008/0004573.

Acknowledgment. Author contributions: H. Jo, J. Mužík, and Y. Koshiba conducted the mathematical derivation. H. Jo, M. Sawicka-Chyla carried out simulation. K. Hashimoto designed optical element. H. Jo, P. Sikocinski, Y. Levy and J. Mužík analyzed material property. P. Sikocinski, Y. Levy and J. Mužík carried out the experiment. H. Jo wrote the manuscript. H. Jo, J. Mužík, P. Sikocinski and M. Chyla analyzed the data. M. Smrž and T. Mocek provided the technical guidance and research supervision. All authors contributed to the data collection, discussed the results, and reviewed the manuscript.

Disclosures. The authors declare no conflicts of interest.

Data Availability Statement. The data that support the findings of this study are openly available in Zenodo

Supplemental document. See Supplement 1 for supporting content.

References

1. C. Zhao, J. Degallaix, L. Ju, *et al.*, “Compensation of strong thermal lensing in high-optical-power cavities,” *Phys. Rev. Lett.* **96**, 231101 (2006).
2. H. S. Brandi, “Excitations of laser states in a cw Ar^{3+} laser,” *Phys. Rev. Lett.* **29**, 1539–1541 (1972).
3. L. Shaughnessy, R. E. McIntosh, A. Goetschy, *et al.*, “Multiregion light control in diffusive media via wavefront shaping,” *Phys. Rev. Lett.* **133**, 146901 (2024).
4. A. Ozawa, T. Udem, U. D. Zeilner, *et al.*, “Modeling and optimization of single-pass laser amplifiers for high-repetition-rate laser pulses,” *Phys. Rev. A* **82** (2010).
5. C. Neuville, C. Baccou, A. Debayle, *et al.*, “Spatial and transient effects during the amplification of a picosecond pulse beam by a nanosecond pump,” *Phys. Rev. Lett.* **117** (2016).
6. J. Speiser, “Scaling of thin-disk lasers—influence of amplified spontaneous emission,” *J. Opt. Soc. Am. B* **26**, 26 (2009).
7. A. Antognini, K. Schuhmann, F. D. Amaro, *et al.*, “Thin-disk Yb:YAG oscillator-amplifier laser, ASE, and effective Yb:YAG lifetime,” *IEEE J. Quantum Electron.* **45**, 993–1005 (2009).
8. W. Zhao, G. Zhu, Y. Chen, *et al.*, “Numerical analysis of a multi-pass pumping Yb:YAG thick-disk laser with minimal heat generation,” *Appl. Opt.* **57**, 5141 (2018).
9. S. Radmard, S. Arabgari, and M. Shayganmanesh, “Optimization of Yb:YAG thin-disk-laser design parameters considering the pumping-light back-reflection,” *Opt. Laser Technol.* **63**, 148–153 (2014).
10. S. Radmard, A. Moshaii, and K. Pasandideh, “400 W average power q-switched Yb:YAG thin-disk-laser,” *Sci. Rep.* **12**, 16918 (2022).
11. K. Contag, M. Karszewski, C. Stewen, *et al.*, “Theoretical modelling and experimental investigations of the diode-pumped thin-disk Yb : YAG laser,” *Quantum Elec. (Woodbury)* **29**, 697–703 (1999).
12. J. Dong and P. Deng, “Temperature dependent emission cross-section and fluorescence lifetime of Cr,Yb:YAG crystals,” *J. Phys. Chem. Solids* **64**, 1163–1171 (2003).
13. J. Koerner, C. Vorholt, H. Liebetrau, *et al.*, “Measurement of temperature-dependent absorption and emission spectra of Yb:YAG, Yb:LuAG, and Yb:CaF₂ between 20 °C and 200 °C and predictions on their influence on laser performance,” *J. Opt. Soc. Am. B* **29**, 2493 (2012).
14. X. Délen, F. Balembois, and P. Georges, “Temperature dependence of the emission cross section of Nd:YVO₄ around 1064 nm and consequences on laser operation,” *J. Opt. Soc. Am. B* **28**, 972 (2011).
15. Y. Sato and T. Taira, “Temperature dependencies of stimulated emission cross section for Nd-doped solid-state laser materials,” *Opt. Mater. Express* **2**, 1076 (2012).
16. S. Chénais, F. Druon, S. Forget, *et al.*, “On thermal effects in solid-state lasers: The case of ytterbium-doped materials,” *Prog. Quantum Electron.* **30**, 89–153 (2006).
17. J. Liao, Y. Lin, Y. Chen, *et al.*, “Flux growth and spectral properties of Yb:YAB single crystal with high yb^{3+} concentration,” *J. Cryst. Growth* **267**, 134–139 (2004).
18. T. Taira, W. M. Tulloch, and R. L. Byer, “Modeling of quasi-three-level lasers and operation of cw Yb:YAG lasers,” *Appl. Opt.* **36**, 1867–1874 (1997).
19. N. Hodgson and H. Weber, *Laser resonators and beam propagation*, Springer series in optical sciences (Springer, New York, NY, 2005), 2nd ed.
20. M. Seidel, L. Lang, C. R. Phillips, and U. Keller, “Influence of disk aberrations on high-power thin-disk laser cavities,” *Opt. Express* **30**, 39691–39705 (2022).
21. T. Dietrich, C. Röcker, T. Graf, and M. Abdou Ahmed, “Modelling of natural convection in thin-disk lasers,” *Appl. Phys. B* **126** (2020).
22. J. Körner, V. Jambunathan, J. Hein, *et al.*, “Spectroscopic characterization of yb^{3+} -doped laser materials at cryogenic temperatures,” *Appl. Phys. B* **116**, 75–81 (2013).
23. U. Demirbas, M. Kellert, J. Thesinga, *et al.*, “Advantages of YLF host over YAG in power scaling at cryogenic temperatures: direct comparison of Yb-doped systems,” *Opt. Mater. Express* **12**, 2508 (2022).
24. J. Dong, M. Bass, Y. Mao, *et al.*, “Dependence of the Yb^{3+} emission cross section and lifetime on temperature and concentration in yttrium aluminum garnet,” *J. Opt. Soc. Am. B* **20**, 1975 (2003).
25. “ISO 11146-1:2021,” *Tech. rep.* (2021). Accessed: 2025-8-21.
26. M. H. Griessmann, A. C. Martinez-Becerril, and J. S. Lundeen, “A method to determine the M^2 beam quality from the electric field in a single plane,” *Opt. Contin.* **2**, 1833 (2023).
27. P. Peterson, A. Gavrielides, T. C. Newell, *et al.*, “ASE in thin disk lasers: theory and experiment,” *Opt. Express* **19**, 25672 (2011).

Unified analysis of spatially-coupled absorption and saturation dynamics in multi-pass pumped disk lasers

HANJIN JO,^{1,*} JIŘÍ MUŽÍK,¹ PAWEŁ SIKOCINSKI,¹ MAGDALENA SAWICKA-CHYLA,¹ MICHAŁ CHYLA,¹ YUYA KOSHIBA,¹ YOANN LEVY,¹ KOHEI HASHIMOTO,¹ MARTIN SMRŽ,¹ AND TOMÁŠ MOCEK¹

¹HiLASE Centre, Institute of Physics of the Czech Academy of Sciences, Za Radnicí 828, 252 41 Dolní Břežany, Czech Republic

*hanjin.jo@hilase.cz

A. Derivation of Effective Absorption Coefficient from Quasi-Three-Level Rate Equation

Steady-State Population Inversion

The population inversion ratio in a quasi-three-level system is governed by the rate equation:

$$\frac{d\beta}{dt} = -\gamma_{12}\beta + [(\sigma_{\text{abs}}^p(1-\beta) - \sigma_{\text{em}}^p\beta)\Phi_p + (\sigma_{\text{abs}}^l(1-\beta) - \sigma_{\text{em}}^l\beta)\Phi_l] \quad (1)$$

where the normalized population inversion is defined as:

$$\beta = \frac{N_2}{N_0} \quad (\text{population inversion ratio}) \quad (2)$$

$$\Phi_p = \frac{I_p}{h\nu_p} \quad (\text{pump photon flux}) \quad (3)$$

$$\Phi_l = \frac{I_l}{h\nu_l} \quad (\text{signal photon flux}) \quad (4)$$

$$\gamma_{12} = \frac{1}{\tau_{21}} \quad (\text{spontaneous decay rate}) \quad (5)$$

Saturation Intensity and Absorption

At steady state, $\frac{d\beta}{dt} = 0$, the rate equation simplifies to a monochromatic case:

$$0 = -\gamma_{12}\beta + (\sigma_{\text{abs}}(1-\beta) - \sigma_{\text{em}}\beta)\Phi \quad (6)$$

Saturation occurs when the stimulated transition rate equals the decay rate:

$$(\sigma_{\text{abs}} + \sigma_{\text{em}})\Phi_{\text{sat}} = \gamma_{12} \quad (7)$$

Converting to intensity, the saturation intensity is defined as:

$$I_{\text{sat}} = h\nu\Phi_{\text{sat}} = \frac{h\nu\gamma_{12}}{\sigma_{\text{abs}} + \sigma_{\text{em}}} \quad (8)$$

Consequently, the effective absorption coefficient exhibits saturable behavior:

$$\alpha_{\text{eff}} = \frac{\alpha_0}{1 + \frac{I_p}{I_{\text{sat}}}} \quad (9)$$

Multipass Propagation and Overlapped Intensity

For multipass configurations, the overlapped transmitted energy is:

$$E_{\text{eff}} = E_0 e^{-\alpha_{\text{eff}} L} \sum_{k=0}^{n_{\text{pass}}-1} e^{-k \alpha_{\text{eff}} L} = E_0 e^{-\alpha_{\text{eff}} L} \frac{1 - e^{-n_{\text{pass}} \alpha_{\text{eff}} L}}{1 - e^{-\alpha_{\text{eff}} L}} \quad (10)$$

The overlapped intensity is related to the incident pump intensity as:

$$I_{\text{eff}} = I_p \cdot \frac{e^{-\alpha_{\text{eff}} L} (1 - e^{-n_{\text{pass}} \alpha_{\text{eff}} L})}{(1 - e^{-\alpha_{\text{eff}} L})} \quad (11)$$

Self-Consistent Effective Absorption Coefficient

Substituting Eq. (11) into Eq. (9), the effective absorption coefficient is implicitly defined by:

$$\alpha_{\text{eff}} = f(\alpha_{\text{eff}}, I_p) = \frac{\alpha_0}{1 + I_p \cdot \frac{e^{-\alpha_{\text{eff}} L} (1 - e^{-n_{\text{pass}} \alpha_{\text{eff}} L})}{I_{\text{sat}} (1 - e^{-\alpha_{\text{eff}} L})}} \quad (12)$$

where the fixed-point equation is:

$$\alpha_{\text{eff}}^* = f(\alpha_{\text{eff}}^*, I_p) \quad (13)$$

with the domain constraints $\alpha_0 > 0$, $n_{\text{pass}} \geq 1$, and $I_p > 0$.

B. Existence and Uniqueness of the Fixed Point

We prove the existence and uniqueness of the effective absorption coefficient α_{eff}^* by establishing three key properties of $f(\alpha, I_p)$:

I. Continuity

The function $f(\alpha, I_p)$ is composed of continuous exponential and rational terms for all $\alpha > 0$. Since the denominator $(1 - e^{-\alpha L}) > 0$ is always positive, f remains bounded and continuous on any interval $[\varepsilon, \alpha_0]$ for $\varepsilon > 0$. Furthermore, all terms are positive, ensuring:

$$0 < f(\alpha, I_p) \leq \alpha_0 \quad \text{for all } \alpha \in (0, \alpha_0] \quad (14)$$

This implies $f([\varepsilon, \alpha_0], I_p) \subseteq [\varepsilon, \alpha_0]$, satisfying the condition for a contractive mapping.

II. Monotonicity

Differentiating $f(\alpha, I_p)$ with respect to α :

$$\frac{\partial f}{\partial \alpha} = \frac{\alpha_0}{[1 + I_p \cdot \mathcal{T}(\alpha)]^2} \cdot \left(-I_p \frac{\partial \mathcal{T}}{\partial \alpha} \right) \quad (15)$$

where $\mathcal{T}(\alpha) = \frac{e^{-\alpha L} (1 - e^{-n_{\text{pass}} \alpha L})}{I_{\text{sat}} (1 - e^{-\alpha L})}$.

The denominator of \mathcal{T} increases monotonically with α , causing $f(\alpha, I_p)$ to be strictly decreasing:

$$\frac{\partial f}{\partial \alpha} < 0 \quad \text{for all } \alpha \in (0, \alpha_0) \quad (16)$$

III. Boundary Conditions and Intermediate Value Theorem

At $\alpha \rightarrow 0^+$:

$$f(0^+, I_p) \approx \frac{\alpha_0}{1 + \frac{I_p}{I_{\text{sat}}} n_{\text{pass}}} > 0 \quad \Rightarrow \quad f(0^+) - 0 > 0 \quad (17)$$

At $\alpha = \alpha_0$:

$$f(\alpha_0, I_p) = \frac{\alpha_0}{1 + I_p \cdot \frac{e^{-\alpha_0 L} (1 - e^{-n_{\text{pass}} \alpha_0 L})}{I_{\text{sat}} (1 - e^{-\alpha_0 L})}} < \alpha_0 \quad \Rightarrow \quad f(\alpha_0) - \alpha_0 < 0 \quad (18)$$

By the Intermediate Value Theorem, there exists at least one $\alpha^* \in (0, \alpha_0)$ satisfying:

$$f(\alpha^*, I_p) = \alpha^* \quad (19)$$

IV. Uniqueness

Define $g(\alpha) = f(\alpha, I_p) - \alpha$. From Eq. (16):

$$\frac{dg}{d\alpha} = \frac{\partial f}{\partial \alpha} - 1 < -1 < 0 \quad (20)$$

Since $g(\alpha)$ is strictly decreasing, the equation $g(\alpha) = 0$ has at most one solution. Combined with the existence result from the Intermediate Value Theorem, we conclude that there exists exactly one fixed point $\alpha_{\text{eff}}^*(I_p) \in (0, \alpha_0)$.

V. Pump Intensity Dependence

Differentiating the fixed-point equation with respect to I_p :

$$\frac{\partial f}{\partial I_p} = -\frac{\alpha_0 \cdot \mathcal{T}(\alpha)}{[1 + I_p \mathcal{T}(\alpha)]^2} < 0 \quad (21)$$

This demonstrates that α_{eff}^* decreases with increasing pump intensity, consistent with saturable absorption physics: stronger pumping leads to greater spectral saturation and reduced effective absorption.

Conclusion

There exists a unique effective absorption coefficient:

$$\boxed{\alpha_{\text{eff}}^*(I_p) = f(\alpha_{\text{eff}}^*(I_p), I_p)} \quad (22)$$

that characterizes the steady-state pump propagation through the multipass laser medium under saturation conditions. This self-consistent formulation ensures physically realizable solutions that accurately capture the interplay between pump depletion and saturable absorption.